Biomacromolecules

Open Access

pubs.acs.org/Biomac

Article

One-Year Ultralong Intravitreal Release of Tyrosine Kinase Inhibitor from Supramolecular Temperature-Responsive Hydrogel

Xinxin Zhao,[‡‡] Qianyu Lin,[‡‡] Ivan Seah, Queenie Shu Woon Tan, Rubayn Zhi Rong Goh, Karishma N. Mehta, Zengping Liu, Abigail Tan, Sheen Enn Ariel How, Belynn Sim, Pablo Mota-Santiago, Nigel Kirby, Yihao Leow, Chen Chuan Lim, Yi Jian Boo, Shermin S. Goh, Jason Y. C. Lim,* Xian Jun Loh,* and Xinyi Su*

Cite This: *Biomacromolecules* 2025, 26, 8452−8464

Read Online

ACCESS | Metrics & More | Article Recommendations | Supporting Information

ABSTRACT: Retinal neovascular diseases, a leading cause of blindness, can be treated with intravitreal tyrosine kinase inhibitors (TKIs). Injectable intravitreal depots capable of sustained TKI release for more than 6 months are highly desirable. While existing platforms utilize covalently cross-linked hydrogels for prolonged release, thermoreversible hydrogels with good injectability have been deemed unsuitable for long-duration drug delivery due to rapid erosion from weak physical cross-linking. Here, we report the first injectable supramolecular hydrogel capable of 1-year sustained TKI release, prepared by codissolving an amphiphilic thermogel with the TKI. This hydrogel achieved a 12-fold longer drug-release duration compared to commercial Pluronic-F127 thermogel, arising from strong polymer-drug interactions resulting in a distinct gel microstructure and enhanced persistence. The released TKI retained bioactivity after one year, successfully resolving choroidal neovascularization (CNV) lesions in murine models. Our findings highlight the potential of supramolecular hydrogels for ultralong drug delivery to the retina.

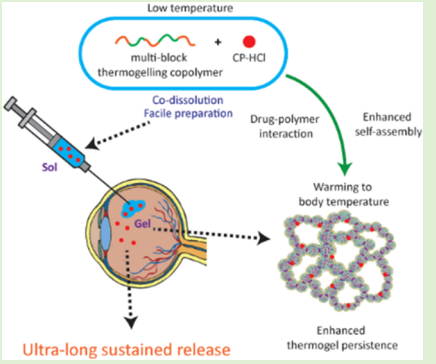

1. INTRODUCTION

Retinal neovascularization, a complication of diseases such as proliferative diabetic retinopathy (DR)[1] and age-related macular degeneration (AMD),[2] is a major cause of blindness.[3,4] Currently, clinical treatment for retinal neovascularization commonly involves regular intravitreal injections of antivascular endothelial growth factors (anti-VEGFs).[5] However, up to 30% of AMD patients do not respond to this treatment.[6,7] Tyrosine kinase inhibitors (TKIs), including pazopanib,[8] regorafenib,[9] PAN90806,[10] and vorolanib,[11] are under clinical investigation as they have the potential to address the issue of nonresponders. For retinal delivery of TKIs, systemic, topical, and intravitreal administration methods have been attempted. However, each method is associated with unique delivery challenges. Topical eye drops have short corneal residence time and poor penetration, limiting the maximal drug concentration at the retina.[12] Meanwhile, systemically delivered TKIs are associated with systemic side effects and face the challenge of achieving adequate vitreous drug concentration due to limited blood supply.[12,13] While intravitreal injections enable direct delivery of TKIs to the retina,[14] frequent injections are associated with poor treatment compliance and sight-threatening complications, including endophthalmitis and retinal detachment.[15]

Sustained-release intravitreal depots are being developed to address the above-stated challenge.[16] Both EYP-1901, a polymer implant capable of achieving therapeutic-relevant vorolanib concentrations,[17] and OTX-TKI, a hydrogel releasing axitinib,[18] are currently undergoing late-stage clinical trials. However, initial results suggest that patients have to resume supplemental anti-VEGF injections after 6 months.[19,20] Furthermore, while these implants offer small-needle injection and biodegradability,[21,22] they suffer from high burst release and solvent toxicity.[23] Therefore, new platforms with longer release and better injectability are needed. Temperature-responsive hydrogels (thermogels) show promise due to biocompatibility, ease of injection, and biodegradability.[24−27] These amphiphilic polymer hydrogels undergo sol−gel transitions upon heating without chemical cross-linkers,[28,29] but their fast erosion limits their use for ultralong (>6 months) drug delivery compared to covalently cross-linked hydrogels.[30,31]

Herein, we report the first supramolecular, injectable thermogel formulation enabling ultralong intravitreal release

Received: June 24, 2025
Revised: August 21, 2025
Accepted: August 21, 2025
Published: November 13, 2025

https://doi.org/10.1021/acs.biomac.5c01212
Biomacromolecules 2025, 26, 8452−8464

of up to one year of the TKI compound, CP-547,632 (CP-HCl), an isothiazole-containing ATP-competitive kinase inhibitor that inhibits VEGF-induced angiogenesis.[32] The antineovascularization effects of systemically delivered CP-HCl have been evaluated in tumor and corneal models, demonstrating up to 85% tumor inhibition in mice and reduced corneal angiogenesis.[32] CP-HCl, delivered topically as PAN90806 has also been evaluated to be safe and well tolerated in early stage clinical trials.[10]

In this work, CP-HCl was physically mixed with an aqueous solution of a thermogelling multiblock copolymer (named EPC), which comprises poly(ethylene glycol) (PEG), poly(propylene glycol) (PPG), and poly(ε-caprolactone) (PCL). The CP-EPC formulation was injectable at 4 °C and gelled spontaneously at body temperature without cross-linkers. Strong drug-polymer interactions enhanced gel stability, enabling sustained CP-HCl release for one year.

Finally, we demonstrated that CP-HCl released from the EPC thermogel retained its bioactivity throughout the one-year release, as the released CP-HCl inhibited proliferation of human umbilical vascular endothelial cells (HUVECs) *in vitro* and significantly reduced choroidal neovascularization (CNV) lesions in murine models of wet AMD. This CP-EPC thermogel has significant translational potential and highlights a strategy for designing injectable, ultralong-release supramolecular hydrogels via strong drug-gel interactions.

2. EXPERIMENTAL SECTION AND METHODS

2.1. Materials and Reagents. Poly(ethylene glycol) (PEG) of M_n 2050 g mol^{-1}, poly(propylene glycol) (PPG) of M_n 2000 g mol^{-1}, poly(ε-caprolactone)-diol (PCL-diol) of M_n 2000 g mol^{-1}, 1,6-hexamethylene diisocyanate (HMDI) (98%), dibutyltin dilaurate (95%), pluronic-F127, and anhydrous toluene were purchased from Sigma-Aldrich (St. Louis, Missouri). Diethyl ether and ethanol absolute were purchased from VWR Chemicals (Radnor, Pennsylvania). Isopropyl alcohol of CMOS grade was purchased from J. T. Baker, Avantor (Radnor, Pennsylvania). Prewetted regenerated cellulose dialysis membrane with molecular weight cutoff of 3500 Da (Spectra/Por 6) and tetrahydrofuran (THF) of high-performance liquid chromatography (HPLC) grade for gel permeation chromatography (GPC) were purchased from Thermo Fisher Scientific (Carlsbad, CA). Deuterated water (D_2O) and deuterated chloroform ($CDCl_3$) were purchased from Cambridge Isotope Laboratories Incorporation (Massachusetts, MA). The neonatal-derived Human umbilical vascular endothelial cells (HUVECs) cat. no. C2519A and EGM-2 endothelial cell growth medium were purchased from Lonza (Basel, Switzerland). A*STAR IRB approval reference number for the use of HUVECs is 2020−147. Cell Counting Kit-8 (WST-8) assay kit was obtained from DojinDo EU (Kumamoto, Japan). Optimal cutting temperature (OCT) compound (Tissue-Tek) was obtained from Sakura Finetek. Aflibercept was obtained from Bayer Healthcare (Berlin, Germany), and CP-HCl (CP-547,632) was purchased from MedChemExpess (New Jersey) and used as received.

2.2. Synthesis of Poly(PEG/PPG/PCL ether urethane) (EPC). EPC1 and EPC3 refer to copolymers synthesized with 1 and 3 wt % feed PCL-diol, respectively. To synthesize EPC1, 12.0 g of PEG (M_n 2050 g mol^{-1}), 3.00 g of PPG (M_n 2000 g mol^{-1}), and 0.150 g of PCL-diol (M_n 2000 g mol^{-1}) were weighed into a clean 250 mL round-bottom flask. To synthesize EPC3, 12.0 g of PEG, 3.00 g of PPG, and 0.450 g of PCL-diol were weighed. The macromonomer-diols were dissolved in 40 mL of anhydrous toluene at 60 °C and dried by 2 rounds of azeotropic distillation. The slurry obtained was further dried under high vacuum for 1 h at 110 °C. Inert dry argon was introduced into the reaction flask, and 90 mL of anhydrous toluene was added before heating up to 110 °C. 15 μL amount of dibutyltin dilaurate (DBTL) catalyst was added, followed by the required amount of hexamethylene diisocyanate (HMDI); 1.21 and 1.22 mL of HMDI were added to synthesize EPC1 and EPC3, respectively. The polymerization reactions were allowed to run for 1 h and 30 min for EPC1 and EPC3, respectively. Subsequently, the reactions were quenched with the addition of 5 mL of absolute ethanol. The crude copolymer was obtained by precipitating it into 1 L of vigorously stirred anhydrous diethyl ether. The supernatant was decanted, and the crude polymer was dried under a constant flow of compressed air. The crude EPC1 and EPC3 copolymers were separately dissolved in 100 mL of isopropyl alcohol (IPA) of CMOS grade by heating at 60 °C for 15 min. Subsequently, the polymer solutions were poured into dialysis tubings of 3.5 kDa molecular weight cutoff and dialyzed against 5 L of deionized water for 3 days with 2 changes of water per day. The dialyzed polymer solutions were frozen and lyophilized for 5 days to obtain purified EPC1 and EPC3.

2.3. NMR Characterization. The compositions of the EPC copolymers were determined via proton nuclear magnetic resonance (NMR) using a Jeol 500 MHz system at room temperature. Copolymers were dissolved at 10 mg mL^{-1} in deuterated chloroform, and 64 scans were performed per sample. To study interactions between CP-HCl and EPC/F127 micelles, EPC and F127 were dissolved at 4 °C overnight in deuterated water at 10 and 40 mg mL^{-1}, respectively, and CP-HCl was codissolved with the individual micellar solutions such that it was present at 10 mg mL^{-1}. ^{1}H NMR was performed on these CP-HCl micellar samples at room temperature with 64 scans per sample.

2.4. GPC Characterization. Apparent molecular weights of the EPC copolymers were determined by gel permeation chromatography (GPC) using Agilent 1260 Infinity II. The GPC system was equipped with a 1260 Vial-sampler, 1260 Iso- Pump, 1260 Refractive Index Detector (RID), and an Agilent PLgel 5 μm MIXED-D column with a molecular weight range of 200−400,000 Da. The system was circulated with THF of HPLC grade at 1 mL min^{-1} and 40 °C. Monodispersed polystyrene standards were used to obtain a calibration curve. Copolymers samples were injected at 3 mg mL^{-1} and 20 μL for GPC measurements.

2.5. ATR-FTIR Measurements and Analysis. To confirm the successful synthesis of EPC copolymers, the purified and lyophilized EPC copolymers were measured using Fourier transform infrared (FTIR) spectroscopy with attenuated total reflection (ATR) attachment (Bruker Vertex 80v). The transmittance spectra were obtained from 4000 to 400 cm^{-1} at a resolution of 1 cm^{-1} with 64 scans per sample at room temperature.

2.6. *In Vitro* Drug Release and Quantification. CP-HCl was dissolved at 40 mg mL^{-1} in phosphate-buffered saline (PBS) with slight heating to 60 °C. Twenty mg of EPC1, EPC3, and F127 were placed in the individual 1.5 mL centrifuge tubes (triplicates), and 100 μL of CP-HCl solution was added to each tube. The depots were kept at 4 °C for 3 nights with thorough mixing to obtain homogeneous formulations of CP-F127 and CP-EPC1. These are subsequently warmed to 37 °C for 30 min to ensure gel formation. 1 mL of prewarmed fresh PBS at 37 °C was added above each gel depot, and the tubes were kept at 37 °C with shaking at 50 rpm. At selected time intervals, 500 μL of each supernatant was removed and replenished with an equal volume of fresh prewarmed PBS. The collected supernatants were stored at −20 °C for drug concentration quantification. The concentration of released CP-HCl was quantified by measuring its absorbance at 261 nm and comparing it to a standard curve obtained with fresh CP-HCl solutions in the range 0−100 μg mL^{-1}. The LOQ of the standard curve is approximately 6.6 μg/mL.

Thereafter, the release profiles of CP-HCl from the thermogels are analyzed by fitting them into the Ritger-Peppas model

$$\frac{M_t}{M_\infty} = Kt^n \tag{1}$$

where M_t/M_∞ is the fraction of the drug released at time t, K is the rate constant, and n is the release exponent. According to the model and assuming a cylindrical drug reservoir shape,[33] $n \leq 0.45$ indicates that the transport mechanism is dominated by Fickian diffusion, while $0.45 < n < 0.89$ indicates anomalous transport where the rate of drug

https://doi.org/10.1021/acs.biomac.5c01212
Biomacromolecules 2025, 26, 8452−8464

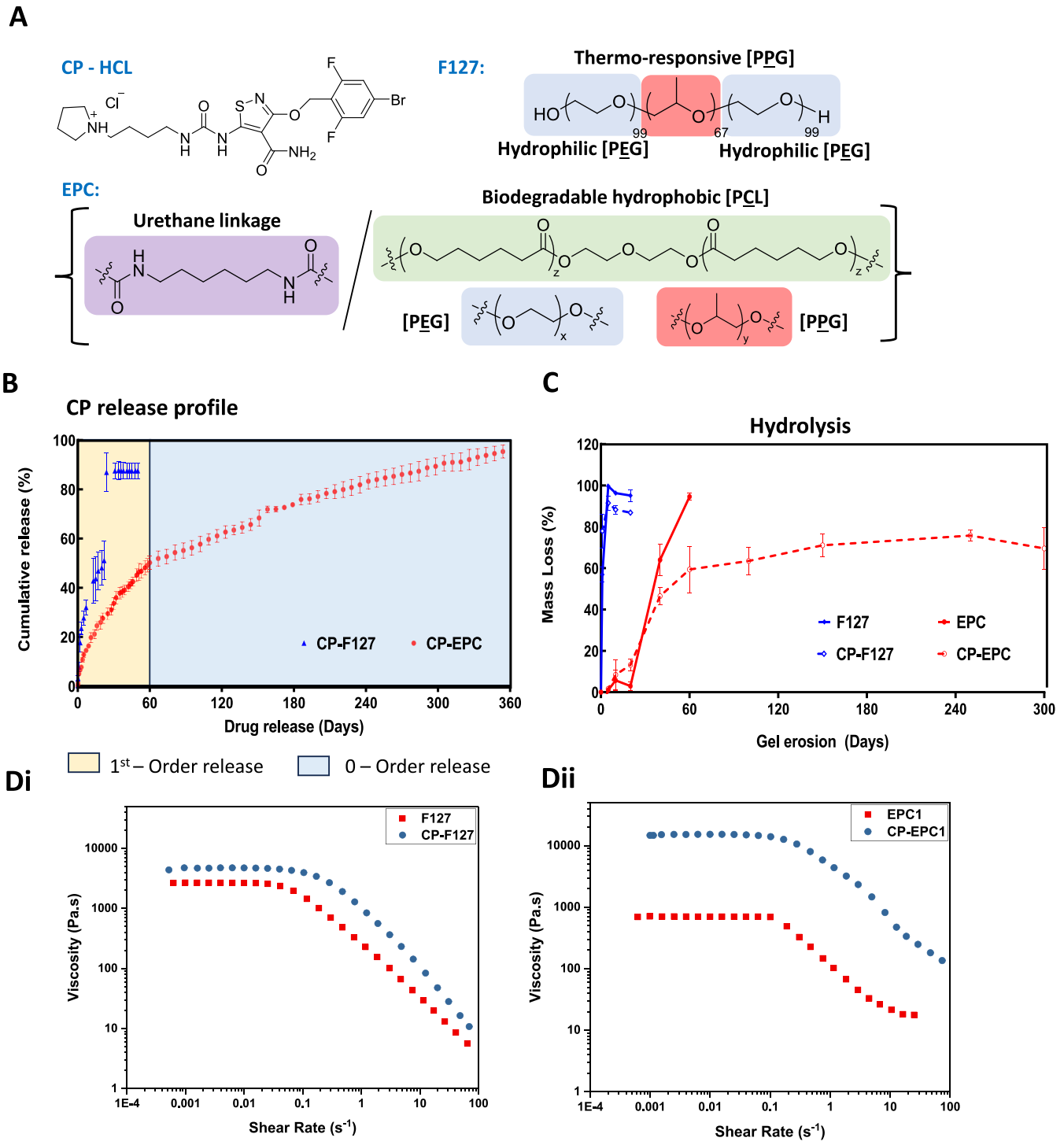

Figure 1. (A) Chemical structures of CP-547,632 hydrochloride (CP-HCl), EPC, and F127. (B) *In vitro* drug-release profiles and (C) gel erosion profiles of CP-EPC and CP-F127. F127 and EPC1 are formulated at 20 wt % while CP-HCl is present at 40 mg mL^{-1}. Data are presented as the mean ± standard deviation (SD) for panels (B, C). All tests were done in triplicates. (D) Viscosity against shear rate rheological measurements of (i) EPC1 and (ii) F127 at 20 wt % before and after mixing with 40 mg mL^{-1} CP-HCl.

diffusion is comparable to the rate of hydrogel matrix relaxation (erosion).[33] Finally, $n \geq 0.89$ indicates relaxation-dominated release, with $n = 1.0$ representing true zero-order release, where the transport is entirely controlled by the erosion of the hydrogel.[33]

2.7. Hydrolytic Degradation of Hydrogel Depots. Preparation of pristine CP-HCl gel depot was done by dissolving 4 mg of it in 100 μL of PBS with slight heating at 60 °C. Pristine EPC1, EPC3, and F127 sols were formed by dissolving 20 mg of each polymer in 100 μL of PBS overnight at 4 °C. CP-EPC1, CP-EPC3, and CP-F127 sols were formed by dissolving 20 mg of each polymer in 100 μL of 40 mg mL^{-1} CP-HCl in PBS at 4 °C for 3 days. All samples were prepared in triplicates. The pristine thermogels and CP-thermogel formulations were warmed to 37 °C for 30 min before 1 mL of fresh PBS was added above the gels. All samples were shaken at 50 rpm. At predetermined time points, the PBS supernatants from each sample were completely removed to collect the remaining gel. The percentage of hydrolytic degradation was defined as

https://doi.org/10.1021/acs.biomac.5c01212
Biomacromolecules 2025, 26, 8452−8464

$$\text{degradation}\ (\%) = (W_0 - W_t)/W_0 \times 100\% \quad (2)$$

where W_0 is the initial mass of polymer and W_t is the mass of the lyophilized polymer obtained from the collected gel at each time point.

2.8. Small-Angle X-ray Scattering (SAXS) Characterization. Formulations of CP-F127 and CP-EPC were prepared at increasing concentrations of CP-HCl. CP-HCl was dissolved in PBS (1 mL) with slight heating at 60 °C to obtain concentrations of 4, 7, and 10 mg mL^{-1}. 0.2 g of F127 (0.2 g) and EPC1 (0.2 g) were separately weighed into Eppendorf tubes with 4 replicates per polymer. To obtain pristine F127 and EPC1 thermogels at 20 wt %, 1 mL of PBS was added to dry F127 and EPC1 copolymers in their separate tubes. To obtain CP-F127 and CP-EPC formulations of increasing CP-HCl concentrations, 1 mL of each CP-HCl solution was added to F127 or EPC copolymers individually. The final formulations were loaded into quartz capillaries (Hilgenberg) in triplicate per formulation. SAXS measurements were conducted with a photon energy of 18.2 keV at a sample-to-detector distance of ∼7000 mm (Australian Synchrotron, SAXS/WAXS Beamline). Data was collected using a Pilatus3−2 M detector (Dectris, Switzerland) and calibrated with silver behenate. Data reduction was performed using the in-house software Scatter-Brain, while the extracted data was analyzed using Igor Pro.

2.9. *In Vitro* Bioactivity of Released CP-HCl. The *in vitro* bioactivity of released CP-HCl was studied based on the viability of human umbilical vascular endothelial cells (HUVEC cells) after 24 h of exposure to the CP-HCl released from the thermogel depots collected at various time points. HUVECs were seeded at a density of 10,000 cells per well in a 96-well plate, and the cells were incubated at 37 °C with 5% CO_2 for at least 20 h to ensure cell adhesion to the plate. The collected CP-HCl solutions (in PBS) were diluted 10 times using cell culture media. Thereafter, the cell culture media in the 96-well plate were aspirated and replaced with 100 μL of diluted CP-HCl solutions per well. After 24 h, the HUVEC viability was quantified using the WST-8 reagent (Cell Counting Kit-8, Dojindo Laboratories, Mashiki, Japan)

2.10. Animal Studies. Male wild-type C57*B*/6J mice, 6 to 8 weeks old, were obtained from In Vivos (Singapore) and used for all *in vivo* experiments. All animal procedures were conducted in accordance with the ARVO Statement on the Use of Animals in Ophthalmic and Vision Research. The experiment was approved by the A*STAR Institutional Animal Care and Use Committee (IACUC): #231751 for a project titled: Testing of therapeutic agents for the ocular delivery of drugs.

2.11. *In Vivo* Bioactivity Assessment of Released CP-HCl. A mouse model of laser-induced choroidal neovascularization (CNV) was used to assess the bioactivity of the released CP-HCl. Mice were first anaesthetized using intraperitoneal ketamine (150 mg kg^{-1}) and xylazine (10 mg kg^{-1}) before photocoagulation was induced in their eyes using an image-guided laser system (Micron IV, Phoenix Research Laboratories, Pleasanton, CA). Seven days later, the mice were anaesthetised again for fundus fluorescein angiography (FFA) using the retinal imaging system (Micron IV, Phoenix Research Laboratories); the photos taken were designated as pretreatment. Thereafter, the mice were divided into 5 groups of 10 eyes: PBS (control), aflibercept (10 mg mL^{-1}), and CP-HCl solutions collected on Day 3, Day 200, and Day 300. Mice from each group were subjected to 1 μL intravitreal injection of the different treatment solutions. After 14 days of postlaser treatment, FFA images were recorded again as post-treatment. The mice were euthanized, and their eyes were enucleated for the preparation of a choroidal flat mount. The enucleated eyes were fixed in 4% paraformaldehyde in PBS overnight at 4 °C. The anterior segment and retina were embedded in paraffin for immunostaining. The eyecups were incubated with isolectin B4 at 4 °C for choroidal vessel staining before 3 cycles of PBS wash. After making four incisions radial to the optic nerve, the tissue was flat-mounted, and Z-stack images of the CNV lesions were taken with the confocal microscope (LSM700, Zeiss, Thornwood, NY).

The FFA and isolectin-staining Z-stack images were imported into ImageJ (US National Institutes of Health, Bethesda, MD). The maximal border of the CNV lesion on each image was manually delineated under magnification, with the area quantified as the number of pixels per 100 μm. The fluorescence intensity of the CNV lesions was graded using ImageJ (National Institutes of Health, Bethesda, MD) by 2 independent graders with single blinding. For FFA quantification, the individual spot pre- and post-treatment samples were recorded and compared. For Isolectin staining, the staining of individual eyes was compared with the average staining from eyes treated by the buffer.

3. RESULTS AND DISCUSSION

3.1. CP-EPC Depot Sustains *In Vitro* Drug Release up to 1 Year with Slow Thermogel Erosion. To prepare the CP-EPC depot, we first synthesized the amphiphilic thermogelling random multiblock copolymer, poly(PEG/PPG/PCL ether urethane) (EPC), via the polyaddition reaction between hexamethylene diisocyanate (HMDI) and the respective macromonomer-diols (Figure S1), which were then purified by dialysis and lyophilization. To facilitate polymer biodegradability and bioresorbability *in vivo*, 1 wt % PCL was incorporated into the polymer (named EPC1) (Figure S1−S3 and Table S1). Proton nuclear magnetic resonance (^{1}H NMR) analysis of EPC1 confirmed successful incorporation of PEG (δ = 3.64 ppm), PPG (1.12 ppm), and PCL-diol (4.04 ppm) (Figure S2 and Table S1) in the copolymer. Polyurethane formation was confirmed through Fourier transform infrared (FTIR) spectroscopy by the presence of urethane stretching at 1650 cm^{-1} in the spectrum of EPC (Figure S4).

The loading of the EPC thermogel with CP-HCl was achieved by first dissolving CP-HCl at 40 mg mL^{-1} in phosphate-buffered solution (PBS) and then dissolving the purified EPC1 copolymer in the CP-HCl solution at 20 wt % at 4 °C for 2 days to form a homogeneous, transparent, viscous sol. The CP-EPC drug-gel depot was subsequently formed by warming the sol to a physiological temperature (Figure 1A). The release of CP-HCl from EPC1 was benchmarked against that from Pluronic F127 (20 wt %), a commercially available polyether triblock copolymer (PEG−PPG-PEG) with well-established applications in sustained drug release[34,35]

CP-HCl is an amphiphilic small molecule[32] and has been shown to self-assemble in water to form a gel at concentrations of 10 mg/mL and above, likely driven predominantly by hydrophobic interactions. Alone, the CP-HCl gel demonstrated sustained drug release for approximately 20 days due to its inherent propensity for self-assembly, which helps to resist immediate erosion and dilution (Figure S5A). CP-HCl was subsequently mixed with EPC1 and F127 to create TKI-thermogel complexes, and their release profiles were monitored over time (Figures 1B and S5A). Our results showed that CP-F127 had a release duration of approximately 20 days, similar to that of CP-HCl gels (Figures 1B and S5A), suggesting that the self-assembled F127 polymer matrix had a minimal impact on delaying the release of CP-HCl. This is supported by the gel erosion profiles, showing that CP-F127 had a gel persistence duration of less than 30 days, comparable to that of gels formed from F127 alone (Figure 1C).

Remarkably, the CP-EPC1 gel depot achieved a significantly longer sustained release of CP-HCl, lasting approximately one year (Figures 1B and S5A). This finding is further supported by the gel erosion profiles, which indicate that CP-EPC1 can persist for about 300 days, much longer than the gel

https://doi.org/10.1021/acs.biomac.5c01212
Biomacromolecules 2025, 26, 8452−8464

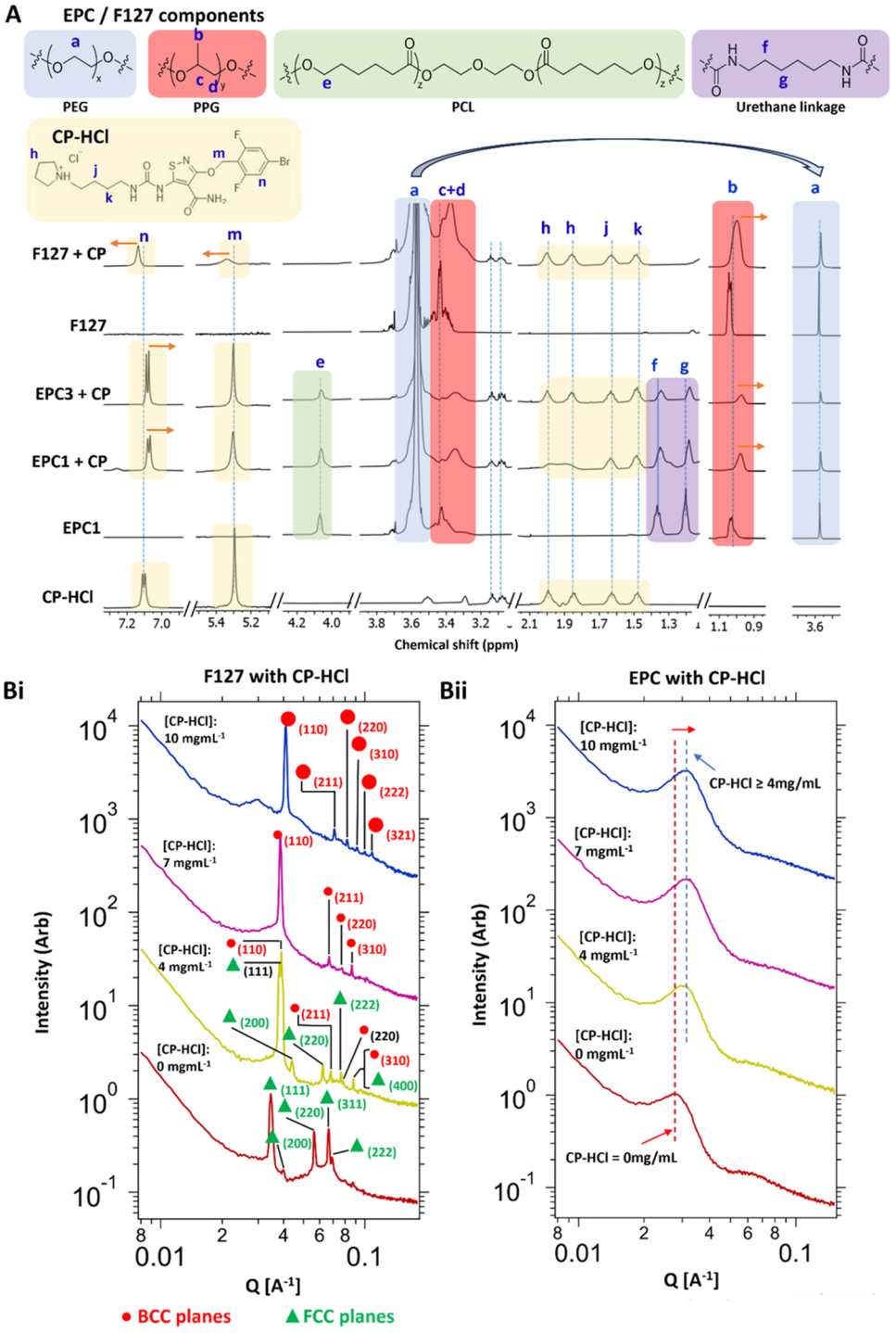

Figure 2. (A) Stacked ^{1}H NMR spectra of CP-HCl (10 mg mL^{-1}), EPC (10 mg mL^{-1}), F127 (40 mg mL^{-1}), and the respective mixtures in D_2O. The various polymeric segments are color-coded and identified in the ^{1}H NMR spectra with the corresponding protons labeled. (B) 1-dimensional indexed small-angle X-ray scattering (SAXS) spectra of (i) F127 and (ii) EPC1 formulated at 20 wt % in PBS with increasing concentration of encapsulated CP-HCl from 0 to 10 mg mL^{-1} at 37 °C.

persistence durations of either CP-HCl or EPC1, each lasting around 60 days (Figures 1C and S5B). The extended duration of sustained release for the multiblock EPC gels appears to be minimally affected by the molecular weight of the polymer or the PCL content. For instance, the analogous EPC3 thermogelling polymer, which has a lower molecular weight (54.1 kDa) than EPC1 (84.2 kDa) but contains 3 wt % PCL, also achieved a similar CP-HCl release duration of about one year, along with a comparable gel persistence duration as the CP-EPC1 depot (Figure S5B). This indicated that CP-HCl forms a supramolecular hydrogel with EPC that exhibits enhanced erosion resistance, indicating a strong synergy between EPC and CP-HCl during gel formation. Notably, the significantly slower release of CP-HCl from EPC gels compared to F127 or CP-HCl alone mitigates the toxicity that can arise when drug concentrations exceed therapeutic

https://doi.org/10.1021/acs.biomac.5c01212
Biomacromolecules 2025, 26, 8452−8464

indices,[36] especially in the case of initial burst releases, while also prolonging the effective lifetime of the drug release depot[37]

To better understand the mechanism of drug release from each thermogel depot, and provide insights on the differences in release behaviors between the EPC and F127 gels, drug-release kinetics were modeled using the Ritger-Peppas model (eq 1),[38] which is relevant for the CP-thermogel swellable soluble polymeric meshes. Fitting the release profile of CP-EPC1 achieved a $n = 1.00$ (Figure S6). The zero-order kinetics indicate that CP-HCl was released gradually from the EPC thermogel via a constant surface erosion process. This ensures that drug concentrations are consistently maintained within the therapeutic index for an extended period, as the amount of drug released is equivalent to the amount of drug being excreted from the tissue.[37] In comparison, CP-EPC3 and CP-F127 had release exponents of $n = 0.619$ and $n = 0.664$, respectively, suggesting that the releases in these samples are based on anomalous transport (combination of Fickian diffusion and surface erosion). This is likely attributed to the weaker hydrogel matrixes formed by EPC3 and F127 as compared to EPC1 due to their lower molecular weights. Additionally, the highest rate constant for CP-HCl release was observed from F127 (12.6 kDa) at 1.94×10^{-4} $Day^{-0.664}$, which can again be attributed to F127's less stable self-assembled hydrogel matrices, leading to subsequently higher rates of gel erosion and drug diffusion.[28]

The presence of CP-HCl improved the mechanical properties of F127 and EPC thermogels considerably. After the addition of CP-HCl, there was a significantly larger increase in gel viscosity (Figure 1Di) and stiffness (Figure S8) at physiological temperature was observed for EPC1 compared to F127 (Figure 1Dii). For instance, the viscosities of EPC1 increased 20-fold, in contrast to only 1.5 times for F127, which is markedly larger than the arithmetic sum of their constituent gels' individual viscosities. This further indicates the substantial differences between the self-assembled gel microstructures of EPC1 and F127 with CP-HCl. Nonetheless, the CP-EPC and CP-F127 gels retained their temperature-responsive gelation behavior, as evidenced by the distinct crossovers of storage moduli (G') with loss moduli (G'') upon warming in oscillatory temperature sweep rheology experiments (Figure S8). This is crucial, as it would allow for good injectability by simply lowering the temperature of the drug-gel depot before implantation while facilitating spontaneous stable depot formation when warmed to physiological temperatures. Notably, the self-assembled CP-HCl gel, on its own, does not display the distinct increase in stiffness upon warming that is characteristic of thermogels; instead, it undergoes a reduction in both G′ and G″ (Figure S7A), as expected due to the thermally driven weakening of the supramolecular interactions responsible for amphiphile gel formation. Like the original EPC and F127 thermogels, the incorporation of CP-HCl preserved the shear-thinning behavior typical of supramolecular hydrogels,[39] with increasing shear rate leading to reduced gel viscosity (Figure 1D) and significant applied external strains resulting in gel collapse and reversion to the sol phase (Figure S9).

3.2. Influences of Thermogels on CP-HCl Sustained Release. The aforementioned results amply suggest that the F127 and EPC polymers interact very differently with the CP-HCl amphiphile despite the superficial similarity of both thermogelling polymers containing PEG and PPG segments. Therefore, the origins of these differences were investigated using ^{1}H NMR spectroscopy to illuminate the polymer-drug interactions at a molecular level and small-angle X-ray scattering (SAXS) to provide insights into the self-assembled microstructures during gelation.

^{1}H NMR experiments performed in D_2O on EPC and F127 polymers, both alone and in the presence of CP-HCl, revealed several notable differences (Figure 2A). Small but detectable upfield shifts in the proton signals corresponding to PPG, PCL, and the alkyl chain of HMDI in EPC were observed with the addition of CP-HCl, while the position of the PEG peak remained almost unchanged. A similar upfield shift was also observed for the PPG peaks in F127 when CP-HCl was complexed with F127 micelles. More significant differences were noted with the aromatic signal of CP-HCl (peak *h*, ∼7.1 ppm) upon interaction with different polymers. While slight upfield shifts of these CP-HCl protons were seen when complexed with EPC1 and EPC3, a prominent downfield shift was noted in the presence of F127. Additionally, the methylene signal *m* of CP-HCl, which is directly adjacent to its aromatic unit, showed downfield perturbation with F127, but not with EPCs. In contrast, the CP-HCl protons in environments close to its cationic hydrophilic pyrrolidinium moiety showed negligible signal shifts, strongly suggesting that hydrophobic interactions primarily accounted for the polymer-drug association. Furthermore, signals *h* and *m* of CP-HCl exhibited considerable broadening in the presence of F127, indicating more restricted molecular motions (*vide infra*), yet they retained their characteristic fine structure with the EPCs despite their upfield shifts. Cumulatively, these differences clearly indicate the various interactions between CP-HCl and both thermogelling polymers, leading to more pronounced differences in the local chemical environments around the aromatic hydrophobic segments of the drug.

To elucidate how differences in interactions with CP-HCl impact polymer self-assembly, we employed small-angle X-ray scattering (SAXS) to probe changes in the microstructures of EPC and F127 gel as CP-HCl incorporation increased. The SAXS spectrum of the gel formed by CP-HCl alone at 10 mg mL^{-1} showed that it forms a supramolecular gel with anisotropic characteristics[40] suggesting a preferential orientation in its internal structure, possibly due to a network of fibrillar arrangements (Figure S10)[41] In contrast, the triblock PEG−PPG-PEG copolymeric structure of F127 self-assembles into spherical micelles with hydrophobic cores that gel through micelle jamming.[42] At a concentration of 20 wt % at 37 °C, F127's SAXS spectrum revealed five distinct peaks corresponding to the (111), (200), (220), (311), and (222) planes of the face-centered cubic (FCC) structure (Figure 2Bi).[43] The identification of these planes was based on the characteristic ratios of q-values matching the permitted reflections of an FCC lattice, confirming the organized and periodic arrangement of the micelles[44]

Upon incorporation of CP-HCl, a phase shift was observed, transitioning the F127 thermogel toward a body-centered cubic (BCC) structure. At an intermediate concentration of CP-HCl (4 mg mL^{-1}), the SAXS spectrum displayed peaks characteristic of both FCC and BCC structures, evidenced by reflections corresponding to the (110), (211), (220), and (310) planes alongside the existing FCC peaks (Figure 2Bi).[44] This coexistence of peaks clearly indicates a transitional phase where micelles are organized in both FCC and BCC configurations under the influence of CP-HCl. At a

https://doi.org/10.1021/acs.biomac.5c01212
Biomacromolecules 2025, 26, 8452−8464

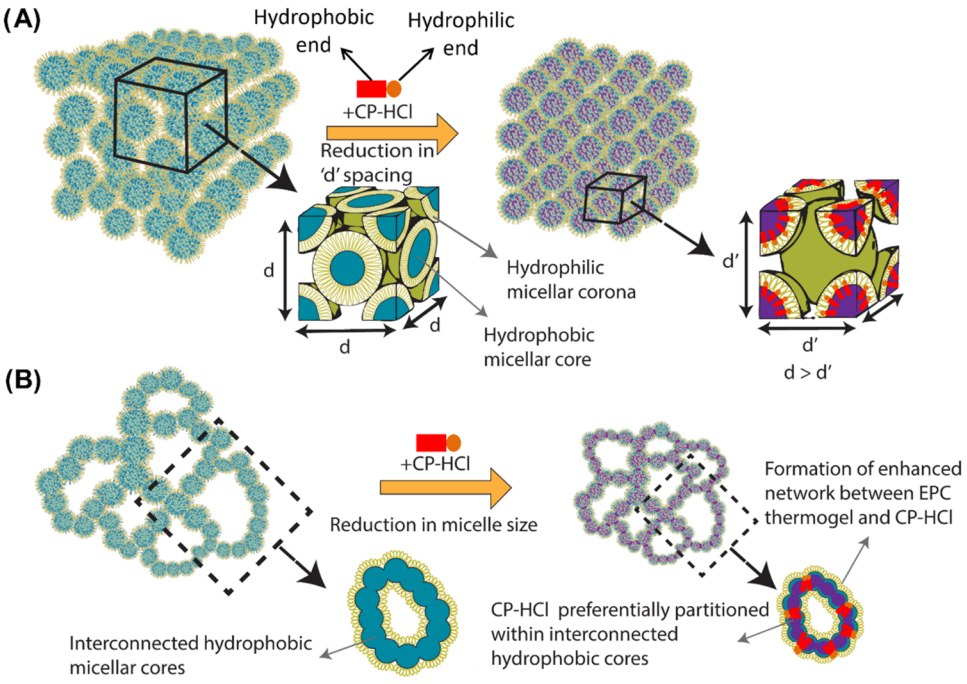

Figure 3. Schematic representation of plausible microstructural changes in (A) F127 and (B) EPC1 thermogels after incorporating CP-HCl.

concentration of 7 mg mL^{-1}, the FCC peaks completely disappeared, with the spectrum showing only BCC reflections, confirming the preferential and exclusive formation of the BCC phase (Figure 2Bi).

This polymorphic behavior is consistent with the reported phase transitions in F127 hydrogels, where the micellar arrangement responds to changes in concentration and external conditions.[45] The lattice parameter, a, can be calculated from the primary q^*, specifically using the (111) reflection for FCC and the (110) reflection for BCC (Table S2).[46] The shift in lattice parameters and the corresponding reduction in micelle sizes (Table S2), observed as the CP-HCl concentration increased, indicate a higher micelle density. This aligns with the proposed mean-field model by Grason, which suggests that BCC is favored at elevated micelle number densities.[47] The hydrophobic nature of CP-HCl likely acts as a driving factor, as it nucleates and stabilizes micelle formation, resulting in lower aggregation numbers and smaller micelles with increased density.[48] This effect has been demonstrated in F127 formulations with hydrophobic drug molecules such as naproxen and indomethacin.[49] In the presence of these drugs, micelle size and aggregation numbers decreased, and the gelation temperature was also lowered.[49] This nucleation effect and stabilization by CP-HCl suggest a mechanism in which the compound shifts the phase preference from FCC to BCC as it compacts the micellar structure.

As a random block copolymer with randomly distributed hydrophobic segments along the polymer chain, EPC gelates through the formation of micellar bridges and interconnected hydrophobic channels.[50,51] The SAXS spectrum of EPC1 shows a prominent broad scattering peak at approximately 0.028 $Å^{-1}$, corresponding to the intermicellar correlation distance (Figure 2Bii).[52] Unlike F127, no higher-order peaks were observed, indicating an absence of long-range periodic order, which is common for thermogels that gelate via the micellar bridging mechanism.[50] With the incorporation of CP-HCl into the EPC thermogel, the prominent broad peak shifted toward higher q with the incorporation of CP-HCl at 4 mg mL^{-1}, but plateaus at approximately 0.31 $Å^{-1}$ above 7 mg mL^{-1} (Figure 2Bii and Table S3). The smaller intermicellar distances observed in the presence of CP-HCl may result from a more compact micelle core and/or an increase in micelle number density, similar to F127.[52] This effect arises from the hydrophobic compartmentalization and stabilization of EPC due to incorporation of the hydrophobic CP-HCl (Figure 3B). The enhanced ability of EPC1 to disperse CP-HCl compared to F127 is evident from a comparison of the 2D-SAXS results at different temperatures, which reveals that F127-CP-HCl formulations exhibit preferential orientation indicative of CP-HCl anisotropy at temperatures of up to 25 °C (Figure S10). This suggests that the encapsulation of CP-HCl by F127 is incomplete at or below this temperature. However, when heated to 37 °C, the encapsulation efficiency of F127 improves, leading to the reestablishment of isotropy. In contrast, EPC consistently achieved effective encapsulation of CP-HCl across all temperatures, even at 5 °C, preventing the formation of anisotropic fibers.

The aforementioned characterizations amply reveal that the different copolymer structures of F127 and EPCs resulted in different CP-HCl encapsulation behaviors, resulting in contrasting gel properties and drug-release durations. The triblock copolymer structure of F127 resulted in distinct spherical micelle formation once above its critical micelle temperature and critical micelle concentration, leading to well-defined encapsulation sites for CP-HCl primarily within the space-constrained hydrophobic micelle cores at 37 °C (Figure 3A). This may explain the noticeable broadening of the aromatic ^{1}H NMR signals from CP-HCl and its adjacent methylene group due to more restricted molecular motions when packed within the micelle cores. The observed transition from FCC to BCC structure by SAXS, along with the higher density of F127-CP-HCl micelle packing, may account for the slight enhancement of the gel mechanical properties. However, the localized encapsulation of CP-HCl within individual

https://doi.org/10.1021/acs.biomac.5c01212
Biomacromolecules 2025, 26, 8452−8464

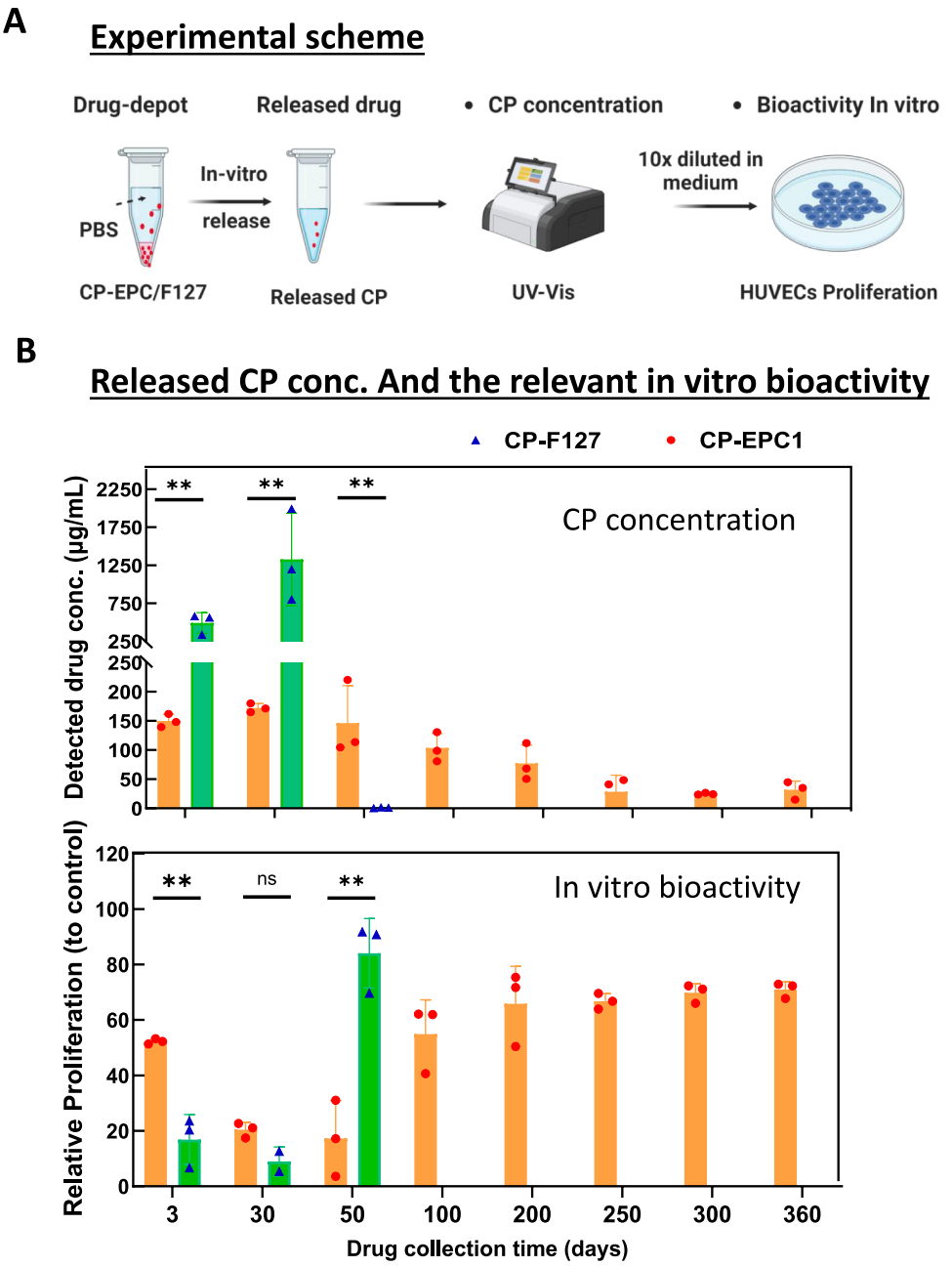

Figure 4. (A) Workflow schematic demonstrating the collection, quantification, and *in vitro* bioactivity assessment of released CP-HCl from CP-F127 and CP-EPC1. (B) Concentration of CP-HCl released from CP-F127 and CP-EPC1 at various time points between 3 and 360 days and their corresponding inhibition of HUVEC proliferation. $n = 3$ for all tests. Statistical analysis: Ordinary one-way ANOVA Multiple comparisons, P value style: GP: 0.1234 (ns), 0.0332 (*), 0.0021 (**), 0.0003 (***), < 0.0001 (****). Data are presented as the mean ± standard deviation (SD).

micelle cores limits their ability to strengthen the overall gel structure and viscosity significantly, resulting in a similar gel persistence duration compared to F127 alone and a short duration of CP-HCl sustained release predominantly governed by gel stability. Conversely, the random distribution of hydrophobic PPG segments within the longer EPC polymers likely enhances their capacity to interact and disrupt the hydrophobic interactions that drive CP-HCl self-assembly, such that effective encapsulation could be observed even at 5 °C by SAXS. As shown by ^{1}H NMR characterizations, the preferential dispersal and partitioning of CP-HCl within the hydrophobic core of EPC's interconnected micellar network contribute to the strengthening of the hydrophobic interactions that facilitate EPC self-assembly (Figure 3B), resulting in tighter networks with smaller intermicellar distances observed from SAXS. Unlike the confined individual hydrophobic cores of F127, the interconnected hydrophobic space of EPC's micellar network can create distinct localized chemical environments and constraints on molecular motion, leading to the unique NMR signal perturbations and a lesser extent of line width broadening of CP-HCl observed with EPC compared to F127. It is feasible that EPC's inability to form distinct micelles like F127, which results in spatially separated, localized sites of CP-HCl encapsulation, facilitates opportunities for synergistic mutual drug-polymer interactions to occur, resulting in the strengthening of the hydrophobic gel network. Ultimately, this leads to enhanced gel stiffness and viscosity, increased gel persistence, and prolonged CP-HCl release from the EPC.

https://doi.org/10.1021/acs.biomac.5c01212
Biomacromolecules 2025, 26, 8452−8464

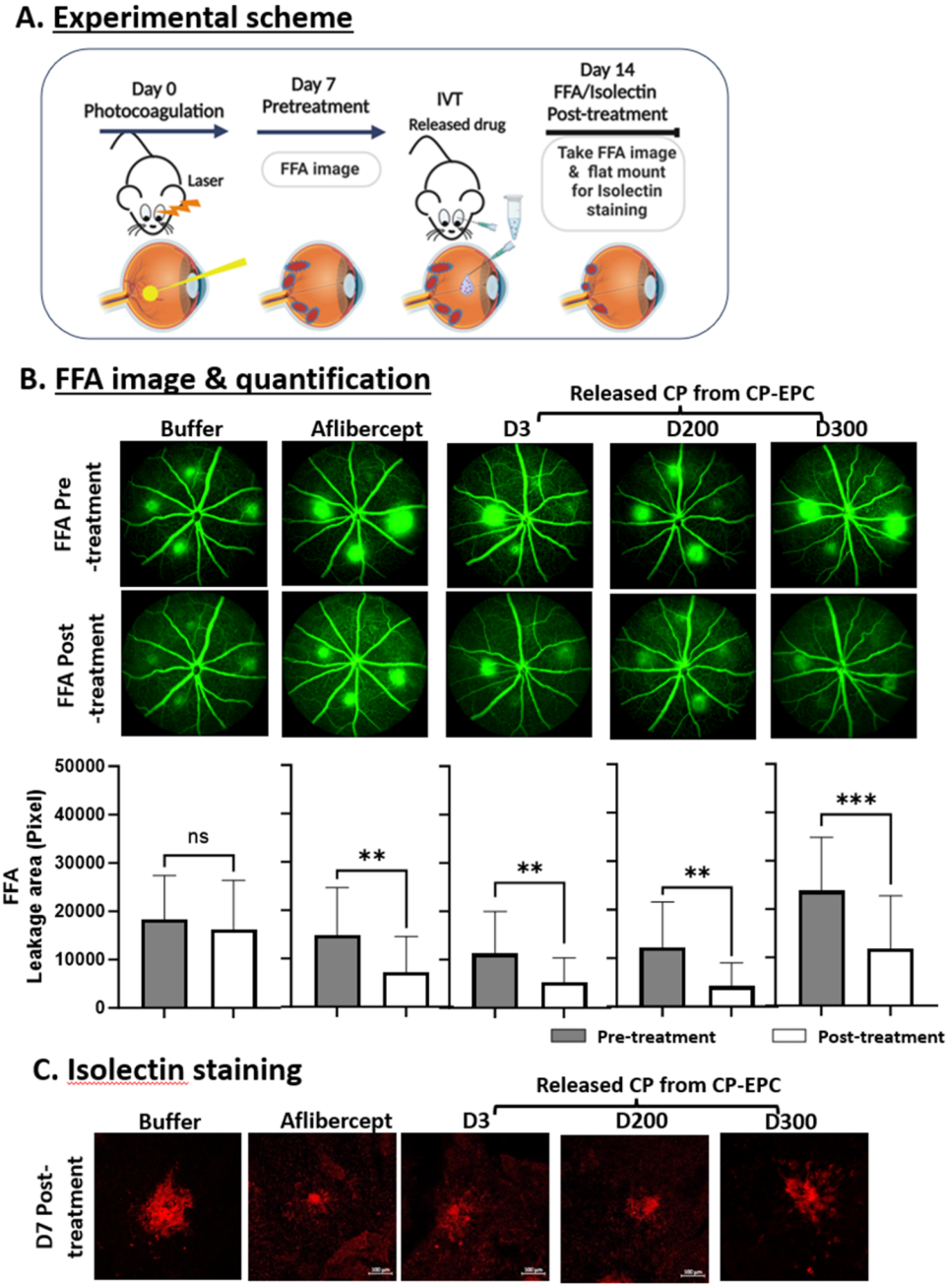

Figure 5. *In vivo* bioactivity assessment of CP-HCl released from the CP-EPC depot in a murine CNV model. (A) Experimental workflow showing the creation of the CNV model, treatment, and assessment procedures for evaluating CP-HCl bioactivity. (B) Fundus fluorescein angiography (FFA) images of murine retina before (top row) and after (bottom row) treatment (PBS, aflibercept, CP-HCl released from CP-EPC at Day 3, Day 200, and Day 300). Green spots represent active CNV lesions. Quantification of CNV lesions is represented in the graph below the representative images. (n = 10 eyes per treatment arm. Data are presented as the mean ± standard deviation (SD).) (C) Isolectin staining images of murine retina 7 days post-treatment (PBS, aflibercept, CP-HCl released from CP-EPC at Day 3, Day 200, and Day 300).

3.3. CP-HCl Released from the EPC−CP Depot Retains Bioactivity. Apart from the sustained release of a drug, it is also important that the released drug maintains its bioactivity throughout its release duration. CP-HCl is a TKI that binds intracellularly to VEGF receptors to exert its antiangiogenic effects. While CP-HCl is a stable small molecule and unlikely to undergo chemical degradation in the mild aqueous environment of the thermogels, the physical interactions between CP-HCl and the thermogelling copolymers can potentially influence its effective bioactivity.[53] As such, the bioactivity of released CP-HCl was assessed by using a human umbilical vein endothelial cell (HUVEC) proliferation assay. As VEGF is a major regulator of HUVEC proliferation,[54] a bioactive CP-HCl molecule would slow the proliferation of these cells. When HUVEC cells were treated with increasing concentrations of CP-HCl (1−10 μg mL^{-1}), the proliferation of the cells was reduced in a concentration-dependent manner (Figure S11). Treatment with a fresh CP-HCl solution at a concentration of 5 μg mL^{-1} resulted in nearly 50% inhibition of HUVEC proliferation. The released CP-HCl from EPC and F127 depots at predetermined time points was subjected to a 10× dilution before being administered to the HUVEC

https://doi.org/10.1021/acs.biomac.5c01212
Biomacromolecules 2025, 26, 8452−8464

proliferation assay (Figure 4A). HUVEC viability was measured after 24 h of incubation. At early time points of Day 3 and Day 30, the concentration of CP-HCl released from CP-F127 was significantly higher than that from CP-EPC due to the rapid erosion of F127 (Figure 4B). The gel-released CP-HCl resulted in relatively lower cell proliferation inhibition compared to freshly prepared CP-HCl (Figure S11), especially significant for the F127 depot at Day 3. This is likely due to a large amount of micelles shed together with CP-HCl, which interfere with drug-receptor interactions.[54] Despite HUVEC viability being inversely correlated with CP-HCl concentration, there was no significant difference in cell viability after treatment with CP-HCl released from EPC and F127 depots collected on Day 30, suggesting that a maximal antiangiogenic effect had been reached, where higher CP-HCl concentrations did not lead to further inhibition of HUVEC proliferation. By Day 50, the CP-F127 depot had nearly completed its release of CP-HCl and, thus, showed minimal inhibition of HUVEC proliferation. In contrast, CP-EPC continued to sustain its release up to Day 360. Throughout this period, released CP-HCl was able to inhibit HUVEC proliferation, suggesting that its bioactivity was well retained by the EPC thermogel depot.

Next, we evaluated the bioactivity of the released CP-HCl from CP-EPC at different time points in reducing vessel leakage using a laser-induced CNV mouse model, which has been a mainstay *in vivo* neovascular AMD model for evaluating therapeutic efficacy.[55] Briefly, a laser is employed to induce damage to the Bruch's membrane of the retina, triggering inflammation and VEGF-driven neovascularization, thereby allowing the model to replicate the pathogenic mechanisms of neovascular AMD. Results generated from this model have been utilized in prior regulatory filings for therapeutic development.

The bioactivity of released CP-HCl from CP-EPC collected on days 3, 200, and 300 was evaluated by injection into CNV mouse models with PBS and aflibercept treatments serving as negative and positive controls, respectively (Figure 5A). To quantify the magnitude of the therapeutic effect, the retinas of CNV mice were imaged using fundus fluorescein angiography (FFA) pre- and post-treatment. FFA is an *in vivo* method to assess the leakage of fluorescein dye, characteristic of neovascularization in the retina (Figure 5B). To ascertain that differences in FFA images were not due to imaging artifacts from the vitreous humor, additional imaging of the retina was performed postenucleation, utilizing isolectin B4 staining to evaluate the CNV lesions (Figure 5C).

In the FFA images, all three CP-HCl treatment arms (Days 3, 200, and 300) demonstrated the reduced intensity of the CNV lesions (green spots) post-treatment. The same qualitative observation was made from the eyes treated with the aflibercept positive control. This was also evident quantitatively, as there was a significant difference between the pre- and post-treatment groups. On average, the sizes of CNV lesions in aflibercept-treated eyes decreased by 51.4%, with the Day 3 treatment arm showing a reduction of 52.8%, the Day 200 treatment arm reducing by 65.5%, and the Day 300 treatment arm reducing by 50.6%, respectively (Figure 5B). Isolectin staining of the choroidal flat mount also revealed smaller CNV lesions in eyes treated with aflibercept compared to those treated with PBS across various treatment arms (Day 3, Day 200, and Day 300). Furthermore, isolectin B4-stained images showed a noticeable difference in CNV lesion size between eyes treated with PBS and those treated with released CP-EPC collected on selected days (Figure 5C). These results suggest that CP-HCl released from CP-EPC maintained its bioactivity and was effective in treating retinal neovascularization.

4. CONCLUSIONS

In summary, we demonstrated an easy-to-formulate injectable supramolecular hydrogel platform that achieves ultralong, sustained delivery of CP-HCl TKI for up to one year. This platform is easy to prepare, requiring only the codissolution of the EPC copolymer with CP-HCl. With the presence of EPC, we observed an over 10-fold increase in the sustained release duration of the drug, along with a concomitant enhancement in gel stiffness, viscosity, and persistence. Extensive characterization experiments show the crucial role of the random block copolymer structure of the EPC depot, leading to synergistic self-assembly behavior of the drug and EPC that strengthens the hydrophobic micellar network, enabling ultralong sustained release. Conversely, the distinct micelles of the commercially available triblock copolymer structure of F127 exhibited contrasting encapsulation behavior, which did not lead to a significantly prolonged drug release. Our EPC multiblock copolymer thermogelling platform is the first supramolecular hydrogel demonstrated for ultralong sustained delivery of TKI, offering significant clinical relevance by reducing injection frequency to once a year while maintaining the drug's therapeutic efficacy. This may improve patient compliance, reduce the risk of infections associated with frequent injections, and lower overall treatment costs. Our work highlights the untapped potential of this overlooked class of easily injectable and formulated platforms for long-duration therapeutic delivery.

■ ASSOCIATED CONTENT

Supporting Information

The Supporting Information is available free of charge at https://pubs.acs.org/doi/10.1021/acs.biomac.5c01212.

Materials pertaining to the synthesis and characterization of the EPC thermogel (PDF)

■ AUTHOR INFORMATION

Corresponding Authors

Jason Y. C. Lim − *Institute of Materials Research and Engineering, Singapore 138634, Singapore; National University of Singapore, Department of Materials Science and Engineering, Singapore 117576, Singapore;* orcid.org/0000-0002-8020-1720; Email: jason_lim@imre.a-star.edu.sg

Xian Jun Loh − *Institute of Materials Research and Engineering, Singapore 138634, Singapore; Nanyang Technological University School of Materials Science and Engineering, Singapore 639798, Singapore; National University of Singapore, Department of Materials Science and Engineering, Singapore 117576, Singapore;* orcid.org/0000-0001-8118-6502; Email: lohxj@imre.a-star.edu.sg

Xinyi Su − *Institute of Molecular and Cell Biology, Singapore 138673, Singapore; National University of Singapore, Department of Ophthalmology, Singapore 119228, Singapore; Singapore Eye Research Institute, Singapore 169856, Singapore; National University Hospital, Department of Ophthalmology, Singapore 119074, Singapore*; Email: xysu@imcb.a-star.edu.sg

https://doi.org/10.1021/acs.biomac.5c01212
Biomacromolecules 2025, 26, 8452−8464

Authors

Xinxin Zhao − *Institute of Molecular and Cell Biology, Singapore 138673, Singapore*

Qianyu Lin − *Institute of Materials Research and Engineering, Singapore 138634, Singapore*

Ivan Seah − *National University of Singapore, Department of Ophthalmology, Singapore 119228, Singapore;* orcid.org/0000-0001-7843-1917

Queenie Shu Woon Tan − *Institute of Molecular and Cell Biology, Singapore 138673, Singapore*

Rubayn Zhi Rong Goh − *Institute of Materials Research and Engineering, Singapore 138634, Singapore;* orcid.org/0000-0001-8333-8143

Karishma N. Mehta − *National University of Singapore, Department of Ophthalmology, Singapore 119228, Singapore*

Zengping Liu − *Institute of Molecular and Cell Biology, Singapore 138673, Singapore; National University of Singapore, Department of Ophthalmology, Singapore 119228, Singapore; Singapore Eye Research Institute, Singapore 169856, Singapore*

Abigail Tan − *National University of Singapore, Department of Biological Sciences, Singapore 117558, Singapore*

Sheen Enn Ariel How − *National University of Singapore, Department of Biological Sciences, Singapore 117558, Singapore*

Belynn Sim − *Institute of Materials Research and Engineering, Singapore 138634, Singapore; Nanyang Technological University School of Materials Science and Engineering, Singapore 639798, Singapore;* orcid.org/0009-0005-8301-150X

Pablo Mota-Santiago − *Australian Synchrotron Co., Ltd., Clayton, Victoria 3168, Australia*

Nigel Kirby − *Australian Nuclear Science and Technology Organisation, Synchrotron, Clayton, Victoria 3168, Australia*

Yihao Leow − *Institute of Materials Research and Engineering, Singapore 138634, Singapore; Nanyang Technological University School of Materials Science and Engineering, Singapore 639798, Singapore*

Chen Chuan Lim − *Institute of Sustainability for Chemicals Energy and Environment, Singapore, Jurong Island 627833, Singapore*

Yi Jian Boo − *Institute of Materials Research and Engineering, Singapore 138634, Singapore*

Shermin S. Goh − *Institute of Materials Research and Engineering, Singapore 138634, Singapore;* orcid.org/0000-0002-8607-3184

Complete contact information is available at: https://pubs.acs.org/10.1021/acs.biomac.5c01212

Author Contributions

‡‡X.Z. and Q.L. contributed equally to this work.

Funding

The authors acknowledge the IAF-PP grant (OrBiTAl: Ocular Biomaterials for Vitreoretinal Therapeutic Applications; Grant number H20c6a0033), National Research Foundation Investigatorship (THETA: Thermogels for Therapeutic Applications; NRF-NRFI07−2021−0003), Clinician Scientist Award by National Medical Research Council (Grant number: MOH-001106), and the A*STAR Central Research Fund for generous funding support for this work.

Notes

The authors declare the following competing financial interest(s): Both X. Su and X.J Loh are non-executive directors and own equity of Vitreogel Innovations Pte Ltd.

■ ACKNOWLEDGMENTS

The authors would like to thank the A*STAR Microscopy Platform (AMP) for providing confocal microscope resources. The authors also acknowledge Dr. Kun Xue for helpful discussions.

■ ABBREVIATIONS

TKI, tyrosine kinase inhibitor; CNV, choroidal neovascularization; DR, diabetic retinopathy; AMD, age-related macular degeneration; VEGF, vascular endothelial growth factor; anti-VEGF, antivascular endothelial growth factors; RTK, receptor tyrosine kinases; ISFI, *in situ* forming implants; CP-HCl, CP-547, 632; PEG, poly(ethylene glycol); PPG, poly(propylene glycol); PCl, poly(ε-caprolactone); HUVEC, human umbilical vascular endothelial cells; EPC, poly(PEG/PPG/PCL ether urethane); 1H NMR, proton nuclear magnetic resonance; FTIR, Fourier transform infrared

■ REFERENCES

(1) Wong, T. Y.; Cheung, C. M.; Larsen, M.; Sharma, S.; Simó, R. Diabetic retinopathy. *Nat. Rev. Dis Primers* **2016**, *2*, No. 16012.

(2) Ratnapriya, R.; Grassman, F.; Chen, R.; Hewitt, A.; Du, J.; Saban, D. R.; Klaver, C. C. W.; Ash, J.; Stambolian, D.; Tumminia, S. J.; Qian, J.; Husain, D.; Iyengar, S. K.; den Hollander, A. I. Functional genomics in age-related macular degeneration: From genetic associations to understanding disease mechanisms. *Exp. Eye Res.* **2025**, *254*, No. 110344.

(3) Wong, W. L.; Su, X.; Li, X.; Cheung, C. M. G.; Klein, R.; Cheng, C.-Y.; Wong, T. Y. Global prevalence of age-related macular degeneration and disease burden projection for 2020 and 2040: a systematic review and meta-analysis. *Lancet Global Health* **2014**, *2* (2), e106−e116.

(4) Teo, Z. L.; Tham, Y.-C.; Yu, M.; Chee, M. L.; Rim, T. H.; Cheung, N.; Bikbov, M. M.; Wang, Y. X.; Tang, Y.; Lu, Y.; Wong, I. Y.; Ting, D. S. W.; Tan, G. S. W.; Jonas, J. B.; Sabanayagam, C.; Wong, T. Y.; Cheng, C.-Y. Global Prevalence of Diabetic Retinopathy and Projection of Burden through 2045: Systematic Review and Meta-analysis. *Ophthalmology* **2021**, *128* (11), 1580−1591.

(5) Wallsh, J. O.; Gallemore, R. P. Anti-VEGF-resistant retinal diseases: a review of the latest treatment options. *Cells* **2021**, *10* (5), No. 1049.

(6) Jiang, D.; Xu, T.; Zhong, L.; Liang, Q.; Hu, Y.; Xiao, W.; Shi, J. Research progress of VEGFR small molecule inhibitors in ocular neovascular diseases. *Eur. J. Med. Chem.* **2023**, *257*, No. 115535.

(7) Lu, C.; Zhang, Q.; Zhang, H.; Li, X.; Jiang, Q.; Yao, J. A small molecular multi-targeting tyrosine kinase inhibitor, anlotinib, inhibits pathological ocular neovascularization. *Biomed. Pharmacother.* **2021**, *138*, No. 111493.

(8) McLaughlin, M.; Bayliffe, A.; Hunt, T.; March, B.; Bailey, C.; Ye, L.; Suttle, B.; Lebowitz, P.; Brigandi, R.; Danis, R. A multi-targeted receptor tyrosine kinase inhibitor for the treatment of neovascular AMD: results of a healthy volunteer safety and tolerability study of pazopanib eye drops. *Invest. Ophthalmol. Visual Sci.* **2009**, *50* (13), No. 5008.

(9) Joussen, A. M.; Wolf, S.; Kaiser, P. K.; Boyer, D. S.; Schmelter, T.; Sandbrink, R.; Zeitz, O.; Boettger, M. K.; Stemper, B. A combined phase 2a/b study of the efficacy, safety, and tolerability of repeated topical doses of regorafenib eye drops in treatment-naïve patients with neovascular age-related macular degeneration (nAMD) *Invest. Ophthalmol. Visual Sci.* 2016; Vol. *57* 12.

(10) Balatsoukas, D. D.; Tsaousis, K. T.; Boboridis, K. G.; Konstas, A. G.; Topouzis, F. Emerging treatment modalities for neovascular age-related macular degeneration: a systematic overview. *Adv. Ther.* **2022**, *39*, 5−32.
(11) Sarkar, A.; Sodha, S. J.; Junnuthula, V.; Kolimi, P.; Dyawanapelly, S. Novel and investigational therapies for wet and dry age-related macular degeneration. *Drug Discovery Today* **2022**, *27* (8), 2322−2332.
(12) Rowe, L. W.; Akotoye, C.; Harris, A.; Ciulla, T. A. Beyond the injection: delivery systems reshaping retinal disease management. *Expert Opin. Pharmacother.* **2025**, *26* (8), 939−952.
(13) Massey, P. R.; Okman, J. S.; Wilkerson, J.; Cowen, E. W. Tyrosine kinase inhibitors directed against the vascular endothelial growth factor receptor (VEGFR) have distinct cutaneous toxicity profiles: a meta-analysis and review of the literature. *Supportive Care Cancer* **2015**, *23*, 1827−1835.
(14) Chandra, S.; Tan, E. Y.; Empeslidis, T.; Sivaprasad, S. Tyrosine Kinase Inhibitors and their role in treating neovascular age-related macular degeneration and diabetic macular oedema. *Eye* **2023**, *37* (18), 3725−3733.
(15) Falavarjani, K. G.; Nguyen, Q. D. Adverse events and complications associated with intravitreal injection of anti-VEGF agents: a review of literature. *Eye* **2013**, *27* (7), 787−794.
(16) Das, N.; Chaurasia, S.; Singh, R. P. A review of emerging tyrosine kinase inhibitors as durable treatment of neovascular age-related macular degeneration. *Expert Opin Emerg Drugs* **2023**, *28* (3), 203−211.
(17) Saim, S.; Sparks, M.; Paggiarino, D.; Karzoun, B. Bioerodible ocular drug delivery insert and therapeutic method. U.S. Patent US17/671,060, 2022.
(18) Khanani, A.; Regillo, C.; Wykoff, C.; Moshfeghi, A.; Weng, C.; Bakri, S. Sustained-release tyrosine kinase inhibitors for the treatment of nAMD. *Retinal Physician* **2022**, *19*, 22−25.
(19) Pharmaceuticals, E.. Phase 2 DAVIO 2 Clinical Trial 12 month Results in wet AMD. https://eyepointpharma.com/trial/phase-2-davio-2-clinical-trial-12-month-results-in-wet-amd/ (accessed January 10, 2025).
(20) Therapeutix, O., Ocular Therapeutix Announces 12-Month Topline Data from Ongoing U.S.-Based Phase 1 Clinical Trial Evaluating OTX-TKI for Treatment of Wet AMD. 2023.
(21) Benhabbour, S. R.; Kovarova, M.; Jones, C.; Copeland, D. J.; Shrivastava, R.; Swanson, M. D.; Sykes, C.; Ho, P. T.; Cottrell, M. L.; Sridharan, A.; et al. Ultra-long-acting tunable biodegradable and removable controlled release implants for drug delivery. *Nat. Commun.* **2019**, *10* (1), No. 4324.
(22) Kovarova, M.; Benhabbour, S. R.; Massud, I.; Spagnuolo, R. A.; Skinner, B.; Baker, C. E.; Sykes, C.; Mollan, K. R.; Kashuba, A. D.; García-Lerma, J. G.; et al. Ultra-long-acting removable drug delivery system for HIV treatment and prevention. *Nature Comm* **2018**, *9* (1), No. 4156.
(23) Maturavongsadit, P.; Paravyan, G.; Kovarova, M.; Garcia, J. V.; Benhabbour, S. R. A new engineering process of biodegradable polymeric solid implants for ultra-long-acting drug delivery. *Int. J. Pharm.: X* **2021**, *3*, No. 100068.
(24) Liow, S. S.; Dou, Q.; Kai, D.; Karim, A. A.; Zhang, K.; Xu, F.; Loh, X. J. Thermogels: In situ gelling biomaterial. *ACS Biomater.* **2016**, *2* (3), 295−316.
(25) Liu, Z.; Liow, S. S.; Lai, S. L.; Alli-Shaik, A.; Holder, G. E.; Parikh, B. H.; Krishnakumar, S.; Li, Z.; Tan, M. J.; Gunaratne, J.; Barathi, V. A.; Hunziker, W.; Lakshminarayanan, R.; Tan, C. W. T.; Chee, C. K.; Zhao, P.; Lingam, G.; Loh, X. J.; Su, X. Retinal-detachment repair and vitreous-like-body reformation via a thermogelling polymer endotamponade. *Nat. Biomed. Eng.* **2019**, *3* (3), 598−610.
(26) Wang, H.; Wang, Q.; Su, Y.; Wang, J.; Zhang, X.; Liu, Y.; Zhang, J. Thermosensitive triblock copolymer for slow-release lubricants under ocular conditions. *ACS Appl. Mater. Interfaces* **2024**, *16* (1), 1675−1687.
(27) Piao, Z.; Lee, H. J.; Jeong, B. Drug-Releasing Thermogel for Osteoarthritis Induction in an Animal Model. *Biomacromolecules* **2023**, *24* (12), 6025−6031.
(28) Lin, Q.; Owh, C.; Lim, Y. C. J.; Chee, P. L.; Yew, P. Y. M.; Hor, T. Y. E.; Loh, X. J. The Thermogel Chronicle—From Rational Design of Thermogelling Copolymers to Advanced Thermogel Applications. *Acc. Mater. Res.* **2021**, *2* (10), 881−894.
(29) Parikh, B. H.; Liu, Z.; Blakeley, P.; Lin, Q.; Singh, M.; Ong, J. Y.; Ho, K. H.; Lai, J. W.; Bogireddi, H.; Tran, K. C.; et al. A bio-functional polymer that prevents retinal scarring through modulation of NRF2 signalling pathway. *Nat. Commun.* **2022**, *13* (1), No. 2796.
(30) Lin, Q.; Ow, V.; Boo, Y. J.; Teo, V. T. A.; Wong, J. H. M.; Tan, R. P. T.; Xue, K.; Lim, J. Y. C.; Loh, X. J. Branched PCL-based thermogelling copolymers: controlling polymer architecture to tune drug release profiles. *Front. Bioeng. Biotechnol.* **2022**, *10*, No. 864372.
(31) Ci, T.; Chen, L.; Yu, L.; Ding, J. Tumor regression achieved by encapsulating a moderately soluble drug into a polymeric thermogel. *Sci. Rep.* **2014**, *4* (1), No. 5473.
(32) Beebe, J. S.; Jani, J. P.; Knauth, E.; Goodwin, P.; Higdon, C.; Rossi, A. M.; Emerson, E.; Finkelstein, M.; Floyd, E.; Harriman, S.; et al. Pharmacological characterization of CP-547,632, a novel vascular endothelial growth factor receptor-2 tyrosine kinase inhibitor for cancer therapy. *Cancer Res.* **2003**, *63* (21), 7301−7309.
(33) Ghosal, K.; Chandra, A.; Rajabalaya, R.; Chakraborty, S.; Nanda, A. Mathematical modeling of drug release profiles for modified hydrophobic HPMC based gels. *Int. J. Pharm. Sci.* **2012**, *67* (2), 147−155.
(34) Nie, S.; Hsiao, W. W.; Pan, W.; Yang, Z. Thermoreversible Pluronic F127-based hydrogel containing liposomes for the controlled delivery of paclitaxel: in vitro drug release, cell cytotoxicity, and uptake studies. *Int. J. Nanomed.* **2011**, 151−166.
(35) Shriky, B.; Kelly, A.; Isreb, M.; Babenko, M.; Mahmoudi, N.; Rogers, S.; Shebanova, O.; Snow, T.; Gough, T. Pluronic F127 thermosensitive injectable smart hydrogels for controlled drug delivery system development. *J. Colloid Interface Sci.* **2020**, *565*, 119−130.
(36) Bhattacharjee, S. Understanding the burst release phenomenon: Toward designing effective nanoparticulate drug-delivery systems. *Ther. Delivery* **2021**, *12* (1), 21−36.
(37) Huang, X.; Brazel, C. S. On the importance and mechanisms of burst release in matrix-controlled drug delivery systems. *J. Controlled Release* **2001**, *73* (2−3), 121−136.
(38) Talevi, A.; Ruiz, M. E. Korsmeyer-Peppas, Peppas-Sahlin, and Brazel-Peppas: Models of Drug Release. In *The ADME Encyclopedia: A Comprehensive Guide on Biopharmacy and Pharmacokinetics*; Springer, 2022; pp 613−621.
(39) Gruschwitz, F. V.; Hausig, F.; Schüler, P.; Kimmig, J.; Hoeppener, S.; Pretzel, D.; Schubert, U. S.; Catrouillet, S.; Brendel, J. C. Shear-Thinning and Rapidly Recovering Hydrogels of Polymeric Nanofibers Formed by Supramolecular Self-Assembly. *Chem. Mater.* **2022**, *34* (5), 2206−2217.
(40) Reyes-Mayer, A.; Alvarado-Tenorio, B.; Romo-Uribe, A.; Benavente, R.; Jaffe, M.; Molina-Ocampo, A. Nanostructure reorganization in a thermotropic copolyester. A simultaneous WAXS and SAXS study. *Polym. Adv. Technol.* **2016**, *27* (6), 748−758.
(41) Sen, D.; Das, A.; Bahadur, J.; Bhatt, H. Time-resolved SAXS investigation on structural evolution of plant fibrillar-network during dehydration. *Surf. Interfaces* **2022**, *29*, No. 101737.
(42) Mortensen, K.; Batsberg, W.; Hvidt, S. Effects of PEO− PPO diblock impurities on the cubic structure of aqueous PEO− PPO− PEO pluronics micelles: fcc and bcc ordered structures in F127. *Macromolecules* **2008**, *41* (5), 1720−1727.
(43) Mandal, M.; Manchanda, A. S.; Zhuang, J.; Kruk, M. Face-centered-cubic large-pore periodic mesoporous organosilicas with unsaturated and aromatic bridging groups. *Langmuir* **2012**, *28* (23), 8737−8745.
(44) Hyde, S. T.Identification of lyotropic liquid crystalline mesophases. In *Handbook of Applied Surface and Colloid Chemistry*; John Wiley & Sons, 2001; Chapter 16, Vol. 2, pp 299−332.

https://doi.org/10.1021/acs.biomac.5c01212
Biomacromolecules 2025, 26, 8452−8464

(45) Bomediano, M. P.; da Silva, L. C.; Mota-Santiago, P.; de Oliveira, M. G.; Plivelic, T. S. Monitoring the micellar packing of photo-crosslinkable Pluronic F127 dimethacrylate during 3D printing. *Front. Soft Matter* **2024**, *4*, No. 1354122.
(46) Lodge, T. P.; Bang, J.; Park, M. J.; Char, K. Origin of the thermoreversible fcc-bcc transition in block copolymer solutions. *Phys. Rev. Lett.* **2004**, *92* (14), No. 145501.
(47) Bang, J.; Lodge, T. P. On the selection of FCC and BCC lattices in poly (styrene-b-isoprene) copolymer micelles. *Macromol. Res.* **2008**, *16*, 51−56.
(48) Basak, R.; Bandyopadhyay, R. Encapsulation of hydrophobic drugs in Pluronic F127 micelles: effects of drug hydrophobicity, solution temperature, and pH. *Langmuir* **2013**, *29* (13), 4350−4356.
(49) Sharma, P. K.; Bhatia, S. R. Effect of anti-inflammatories on Pluronic F127: micellar assembly, gelation and partitioning. *Int. J. Pharm.* **2004**, *278* (2), 361−377.
(50) Cui, S.; Yu, L.; Ding, J. Thermogelling of amphiphilic block copolymers in water: ABA type versus AB or BAB type. *Macromolecules* **2019**, *52* (10), 3697−3715.
(51) Cui, S.; Yu, L.; Ding, J. Semi-bald micelles and corresponding percolated micelle networks of thermogels. *Macromolecules* **2018**, *51* (16), 6405−6420.
(52) Morimura, M.; Ida, S.; Oyama, M.; Takeshita, H.; Kanaoka, S. Design of hydrogels with thermoresponsive crosslinked domain structures via the polymerization-induced self-assembly process and their thermoresponsive toughening in air. *Macromolecules* **2021**, *54* (4), 1732−1741.
(53) Lü, S.; Gao, N.; Cao, Z.; Gao, C.; Xu, X.; Bai, X.; Feng, C.; Liu, M. Pluronic F127−chondroitin sulfate micelles prepared through a facile method for passive and active tumor targeting. *RSC Adv.* **2016**, *6*, 49263−49271.
(54) Soker, S.; Gollamudi-Payne, S.; Fidder, H.; Charmahelli, H.; Klagsbrun, M. Inhibition of vascular endothelial growth factor (VEGF)-induced endothelial cell proliferation by a peptide corresponding to the exon 7-encoded domain of VEGF165. *J. Biol. Chem.* **1997**, *272* (50), 31582−31588.
(55) Lambert, V.; Lecomte, J.; Hansen, S.; Blacher, S.; Gonzalez, M.-L. A.; Struman, I.; Sounni, N. E.; Rozet, E.; De Tullio, P.; Foidart, J. M.; et al. Laser-induced choroidal neovascularization model to study age-related macular degeneration in mice. *Nat. Protoc.* **2013**, *8* (11), 2197−2211.

https://doi.org/10.1021/acs.biomac.5c01212
Biomacromolecules 2025, 26, 8452−8464